HX-ESI-MS and Optical Studies of the Unfolding of Thioredoxin Indicate Stabilization of a Partially Unfolded, Aggregation-Competent Intermediate at Low pH[†]

Ajazul Hamid Wani and Jayant B. Udgaonkar*

National Centre for Biological Sciences, Tata Institute of Fundamental Research, Bangalore 560065, India

Received April 3, 2006; Revised Manuscript Received June 27, 2006

ABSTRACT: Hydrogen exchange monitored by mass spectrometry (HX-MS), in conjunction with multiple optical probes, has been used to characterize the unfolding of thioredoxin. Equilibrium and kinetic studies have been carried out at pH 7 and 3. The HX-MS measurements are shown to be capable of distinguishing between native (N) and unfolded (U) protein molecules when both are present together, and their application in kinetic experiments allows the unfolding reaction to be delineated from the proline isomerization reaction to which it is coupled. At pH 7, equilibrium unfolding studies monitored by three optical probes, intrinsic fluorescence at 368 nm, ellipticity at 222 nm, and ellipticity at 270 nm, as well as by HX-MS, indicate that no intermediate is populated at pH 7, the unfolding reaction is slower than the proline isomerization reaction that follows it, and the three optical probes yield identical kinetics for unfolding, which occurs in a single kinetic phase. The fractional change in any of the three optical signals at any time of unfolding predicts the fraction of the molecules that have become U, as determined by HX-MS. Hence, unfolding at pH 7 appears to occur via a two-state N ⇌ U mechanism. In contrast at pH 3, HX-MS as well as optical measurements indicate that an unfolding intermediate is stabilized and hence accumulates in equilibrium with N and U, at concentrations of denaturant that define the transition zone of the equilibrium unfolding curve. The intermediate has lost the near-UV signal characteristic of N and possesses fewer amide hydrogen sites that are stable to exchange than does N. Kinetic experiments at pH 3, where unfolding is much faster than proline isomerization, show that more than one intermediate accumulates transiently during unfolding. Thus, the unfolding of thioredoxin occurs via an N ⇌ I ⇌ U mechanism, where I is a partially unfolded intermediate that is stabilized and hence populated at pH 3 but not at pH 7. It is shown that transient aggregation of this intermediate results in a deceleration of the kinetics of unfolding at high protein concentrations at pH 3 but not at pH 7.

Obtaining an understanding of how proteins unfold can yield valuable information about protein folding mechanisms. Kinetic unfolding studies have been used to characterize the transition state of protein folding (*1*, *2*), to demonstrate the possibility of multiple pathways for folding and unfolding (*3*−*9*), and to characterize intermediates that may accumulate on unfolding pathways (*3*, *10*−*13*). Measurements of unfolding rates under refolding conditions (*14*) not only indicate the population of partially folded structures but also indicate that the folding mechanisms in urea and guanidine hydrochloride may be different. Equilibrium unfolding studies have been used to establish the possible sequence of events that follow the rate-limiting step in folding (*15*), to show that non-native structures may form during folding and unfolding (*16*), and to show that protein folding and unfolding reactions may incorporate continuous structural transitions (*17*). Single-molecule unfolding studies have also indicated that unfolding may occur in a stepwise manner (*18*−*20*). Computer simulations of protein unfolding have confirmed the occurrence of unfolding intermediates and multiple pathways and helped in the characterization of the transition state (*21*−*23*). The study of protein unfolding has much practical value because native protein may often, especially when destabilized by mutation or by a change in environment, unfold to partially structured forms that misfold to form specific aggregates such as amyloid fibrils that have been implicated in many neurodegenerative diseases (*24*−*26*) as well as the prion diseases (*27*).

Measurements of hydrogen−deuterium (HX)[1] exchange in folded proteins, in partially folded proteins, in protein aggregates, and in proteins undergoing the process of folding or unfolding have been instrumental in delineating mechanisms of protein folding, unfolding, and misfolding (*15*, *28*). When coupled with the high-mass measuring accuracy and sensitivity of modern electrospray ionization (ESI) mass spectrometry (MS), HX measurements become a relatively fast and sensitive method for studying global and regional conformational changes as well as local dynamics (*29*−*31*).

[†] This work was funded by the Tata Institute of Fundamental Research and by the Wellcome Trust.

* To whom correspondence should be addressed. E-mail: jayant@ncbs.res.in. Fax: 91-80-23636662. Telephone: 91-80-23636421.

[1] Abbreviations: HX, hydrogen exchange; MS, mass spectrometry; Trx, *Escherichia coli* thioredoxin in its oxidized form; ESI, electrospray ionization; GdnHCl, guanidine hydrochloride; CD, circular dichroism; NMR, nuclear magnetic resonance.

10.1021/bi060647h CCC: $33.50
Published on Web 08/25/2006

The most important advantage of using HX-MS methods, in which HX is monitored by ESI-MS, compared to HX-NMR methods, is that MS unlike NMR can distinguish between protein conformations that differ in structure and, hence, in the number of protected amide hydrogen sites, when these conformations are present together (*32*−*35*). Moreover, large proteins as well as protein assemblies, even in very small quantities, can be studied easily by HX-MS, but not by HX-NMR. Of course, HX-MS, unlike HX-NMR, has the disadvantage of not being able to provide residue-specific HX information, but this disadvantage can be overcome partially when HX-MS is used along with proteolysis methods (*36*).

Here we report the application of HX-MS methods to the study of the guanidine hydrochloride (GdnHCl)-induced unfolding of the small protein thioredoxin. *Escherichia coli* thioredoxin (Trx) is a two-domain, 108-amino acid protein. The large domain has a $\beta\alpha\beta\alpha\beta$ fold, and the smaller domain has a $\beta\beta\alpha$ fold (*37*). In the past, HX-MS has been used to study conformational changes in oxidized and reduced Trx, as well as in chemically modified variants (*38*−*41*), but not to characterize folding or unfolding pathways. Much is known about the folding mechanism of Trx from optical studies (*42*−*46*). Trx folds via multiple pathways that originate from the establishment of slow proline isomerization equilibria in the unfolded form (*45*, *46*). In the presence of the chaperone, GroEL, folding is channeled along the slowest folding route (*46*). On the other hand, very little work in characterizing the unfolding reaction of the protein has been done. A native-state HX study (*47*) has failed to identify a partially folded form to which the native state may transiently unfold but has suggested that β strands $\beta2-\beta4$, which form the core of the protein in the native state, may participate in residual structure in the unfolded state under native conditions at pH 7.

In this study, multiple structural probes, including HX-MS, have been used to characterize the unfolding reactions of Trx at pH 7 and 3. At pH 7, no intermediate is seen to be populated during unfolding, either transiently during the time course of unfolding or at equilibrium. At pH 3, an intermediate is seen to populate in equilibrium with the native and unfolded protein. This intermediate has lost the near-UV CD signal characteristic of the native protein, and the structure retained in it does not provide protection from HX, at a subset of the 33 amide hydrogens that are protected in the native protein. In kinetic experiments at pH 3, at least two intermediates are seen to be populated transiently when unfolding is carried out in 2.2−2.5 M GdnHCl, but only one kinetic intermediate is detected when unfolding is carried out in 3 M GdnHCl. At high protein concentrations, the kinetic intermediates detected during unfolding appear to aggregate transiently, and consequently, the unfolding rate is seen to be dependent on protein concentration.

MATERIALS AND METHODS

Buffers and Reagents. D_2O, NaOD, DCl, and other buffers were ultrapure-grade from Sigma, and GdnHCl was from U.S. Biochemical Corp. Sodium phosphate (20 or 30 mM) was used as the buffer at pH 7, and 20 or 30 mM glycine was used at pH 3. All pH values were recorded using a Thermo Orion 420 pH meter, and the pH values reported for D_2O buffers are uncorrected for the isotopic effect.

Protein Purification. The procedure for the purification of Trx has been described previously (*46*) . The protein was >95% pure. Purity was checked by SDS−PAGE and by ESI-MS; a single protein with a mass of 11 673.4 Da was observed. Trx concentrations were determined using a molar extinction coefficient of 13 700 M^{-1} cm^{-1}.

Deuteration of Trx and GdnHCl. Deuteration of Trx was carried out by dissolving 1 mg of lyophilized Trx/mL of D_2O at pH 7, heating at 85 °C for 15 min, and then refolding on ice for 15 min and at 25 °C for 30 min. Mass spectrometry indicated an increase in mass of 180 Da over the protonated protein mass of 11 673 Da. GdnHCl was deuterated (to GdnDCl) by dissolving it in D_2O followed by lyophilization; the procedure was repeated three times to ensure complete deuteration.

Fluorescence and Circular Dichroism Spectra. Fluorescence emission spectra were collected on a Fluoromax-3 fluorimeter, upon excitation at 295 nm using a band-pass of 0.3 nm. Circular dichroism spectra were collected on a Jasco 720 spectropolarimeter, using a bandwidth of 1 nm. Cuvettes with path lengths of 0.1 and 1 cm were used for the far-UV (200−250 nm) and near-UV (240−320 nm) circular dichroism measurements, respectively.

Optically Monitored Equilibrium Unfolding Experiments. Equilibrium unfolding of Trx was carried out both at pH 3 and at pH 7 by incubating the protein (~20 μM for far-UV CD measurements and ~5 μM for fluorescence measurements) in different concentrations of GdnHCl at 25 °C for 4 h. Unfolding was monitored by measurement of far-UV CD at 222 nm (1 nm bandwidth) using a Jasco J720 spectropolarimeter and a cuvette with a path length of 0.1 cm, as well as by measurement of fluorescence emission at 368 nm for pH 7 and 360 nm for pH 3, using a Fluoromax-3 fluorimeter. Equilibrium unfolding curves were fitted to a two-state N ⇌ U model (*48*).

Optically Monitored Kinetic Unfolding Experiments. For kinetic studies in which unfolding was monitored by measurement of far-UV CD, at pH 7 and 3, native protein was diluted to a final concentration of 5 μM in unfolding buffer containing a final GdnHCl concentration ranging from 2.2 to 3.5 M. Unfolding was monitored by measurement of far-UV CD at 222 nm using a cuvette with a path length of 1 cm, with the bandwidth and response time set to 1 nm and 1 s, respectively. For kinetic studies in which unfolding at pH 3 was monitored by measurement of near-UV CD at 270 nm, at GdnHCl concentrations ranging from 2.0 to 3.5 M, and using a final protein concentration of 50 μM, a cuvette with a path length of 1 cm was used, with the bandwidth and response time set to 1 nm and 2 s, respectively. All CD data were collected using a Jasco J-720 spectropolarimeter, and in all cases, the dead time of manual mixing was 10 ± 2 s.

For kinetic studies in which unfolding at pH 7 was monitored by measurement of fluorescence at 368 nm upon excitation at 295 nm, manual mixing (mixing dead time of 5 s) of the solutions was carried out directly into a cuvette with a path length of 1 cm in a Fluoromax-3 fluorimeter. For kinetic unfolding studies carried out at pH 3, an SFM-4 stopped-flow machine (Biologic) was used to initiate unfolding, with a mixing dead time of 6.2 ms, at GdnHCl concentrations ranging from 2.2 to 4.0 M. The concentration of the protein during unfolding was 10 μM, and unfolding

was monitored by measurement of fluorescence emission at 360 nm upon excitation at 295 nm.

HX-MS-Monitored Equilibrium Unfolding Experiments. For equilibrium unfolding studies at pH 7, deuterated Trx was diluted to a final concentration of 800 μM protein into native buffer [20 mM sodium phosphate in D_2O (pH 7)] and unfolding buffer [GdnDCl and 20 mM sodium phosphate in D_2O (pH 7)] so that the final concentration of GdnDCl was 2.2, 2.5, or 2.8 M. The reaction mixture was incubated at 25 °C for 4 h. Then, 15 μL of the reaction mixture described above was diluted 10-fold into 135 μL of labeling buffer (50 mM sodium phosphate in H_2O), containing the same concentration of GdnHCl. After labeling had been carried out for 5 s, the exchange reaction was quenched at pH 3 by diluting the sample 10-fold into 1350 μL of quench buffer [50 mM glycine in H_2O (pH 2.8)]. The samples were then processed for mass spectrometry.

For equilibrium unfolding studies at pH 3, deuterated Trx was diluted to a final concentration of 50 μM, with unfolding buffer [30 mM glycine in D_2O (pH 3)] containing 2.2, 2.5, or 2.8 M GdnDCl, and then incubated at 25 °C for 4 h. Then, 100 μL of the incubated solution was diluted 10-fold into 900 μL of labeling buffer [50 mM sodium phosphate in H_2O (pH 7)] containing an identical concentration of GdnHCl. After labeling had been carried out for 5 s, the exchange reaction was quenched at pH 3, by diluting the sample 10-fold into 9 mL of quench buffer [50 mM glycine in H_2O (pH 2.8)]. The samples were then concentrated to 0.5 mL using a 50 mL Amicon stirred cell so that the concentration of protein became ~10 μM and then processed for mass spectrometry.

HX-MS-Monitored Kinetic Unfolding Studies. For kinetic unfolding studies at pH 7 and 3, a pulse labeling methodology was used. Deuterated protein was diluted with unfolding buffer (3.3 M GdnDCl and 20 mM sodium phosphate in D_2O for pH 7 or 30 mM glycine in D_2O for pH 3) to a final protein concentration of 50 μM and 3 M GdnHCl. The mixing dead time was 11 ± 1 s. After different times of unfolding in 3 M GdnDCl, ranging from 11 to 300 s, a 5 s labeling pulse was given by diluting the sample 10-fold into 900 μL of labeling buffer [50 mM sodium phosphate and 3 M GdnHCl in H_2O (pH 7)]. The exchange reaction was quenched by decreasing the pH to 3 via a 10-fold dilution into 9 mL of quench buffer [50 mM glycine in H_2O (pH ~2.8)]. The resultant reduction at pH 3 quenched the HX reaction, and the reduction of the GdnHCl concentration to 0.3 M enabled the protein to refold. The sample was then concentrated to 0.5 mL using an Amicon stirred cell with a 1 kDa cutoff membrane and processed for mass spectrometry.

It was important to demonstrate that the labeling conditions were sufficient to completely label the unfolded protein but not the native protein. When completely unfolded, deuterated protein in 6 M GdnDCl was given the 5 s labeling pulse, and the sample was processed as described below; only two to three deuteriums were found to have remained unexchanged, either because of residual structure in 6 M DCl or because the labeling buffer contained 10% D_2O. When native deuterated protein was given the 5 s labeling pulse and the sample processed in the same way, 33 ± 3 deuteriums were found to have remained unexchanged, showing that the labeling conditions do not affect the conformation of the protein. In every HX-monitored folding experiment, an important control experiment was to dilute deuterated protein directly 10-fold into quench buffer containing H_2O buffer at pH 3. After the sample had been processed in a manner identical to that for the samples for the unfolding experiments, as described below, 33 ± 3 deuteriums were found to have remained unexchanged.

Processing of HX Samples for Mass Spectrometry. All HX samples were processed in an identical manner. Each sample was desalted using a Sephadex G-25 column equilibrated with water at pH 3 (pH adjusted with formic acid), in conjunction with an Akta chromatography system. After incubation for 24 h at 25 °C (from the time of labeling), the samples were analyzed by electrospray mass spectrometry.

ESI Mass Spectrometry. A Micromass Q-TOF Ultima mass spectrometer (ESI-MS) was used. For acquisition of mass spectra, the capillary voltage was set to 3 kV, the desolvation temperature to 150 °C, and the source temperature to 80 °C. No organic solvent was added to the samples, and the spectra were collected in the positive ion mode. Furthermore, before injection of the sample, the injection line was washed with D_2O or H_2O, depending on whether the sample was in D_2O or H_2O. The concentration of Trx in each sample was typically 5 μM, and typically, an ion count of ~75 was obtained in a 1 s data acquisition window. For each sample, data acquired over 100 s were averaged.

Data Analysis. To quantify the relative amounts of deuterated protein with 33 ± 3 protected deuteriums (mass of 11 706 ± 3 Da) and a protonated protein with a mass of 11 673 Da in each sample, the relative amplitudes of the peaks corresponding to the ninth charged state (*m*/*z* 1301.8) were determined. Relative amplitudes were determined either directly from the ion intensities or from fitting Gaussian distributions to the peaks to determine their areas.

Unfolding kinetics monitored by manual mixing fluorescence measurements were fitted to a single-exponential equation, and unfolding kinetics monitored by stopped-flow mixing fluorescence measurements were fitted to a two-exponential equation.

RESULTS

Structure and Stability of Trx at pH 7 and 3. Figure 1 compares the spectroscopic properties as well as stability of Trx at pH 7 to the spectroscopic properties and stability at pH 3. It is seen that the fluorescence spectra (Figure 1A), the far-UV CD spectra (Figure 1B), and the near-UV CD spectra (Figure 1C) of the protein are identical at pH 7 and 3. The far-UV CD spectrum at pH 7 is identical to that reported in earlier studies (*49*, *50*). These results indicate that both the secondary and tertiary structure of Trx are not changed by the change in pH from 7 to 3, and they are in agreement with an earlier study which indicated that Trx remains in its native conformation in 2% acetic acid (*38*). Size exclusion chromatography as well as dynamic light scattering studies (data not shown) indicate that the protein remains monomeric at both pH 7 and 3, at concentrations of 50 and 500 μM. In Figure 1D, it is seen that the far-UV CD-monitored GdnHCl-induced equilibrium unfolding curve of Trx determined at pH 7 completely overlaps that determined at pH 3. In both cases, the midpoint of the equilibrium unfolding transition is at 2.5 M GdnHCl. Thus, far-UV CD-monitored equilibrium unfolding studies suggest that the stability of Trx is the same at pH 7 and 3.

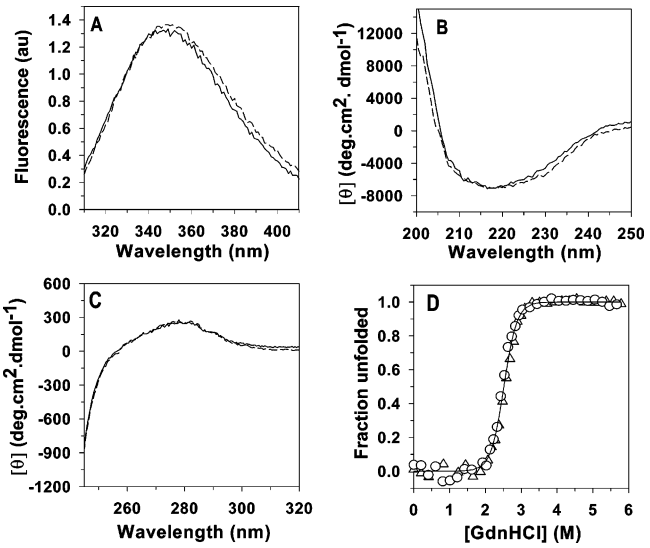

FIGURE 1: Comparison of the structure and stability of thioredoxin at pH 3 and 7. (A) Fluorescence emission spectra of thioredoxin. (B) Far-UV circular dichroism spectra of thioredoxin (18 μM protein). (C) Near-UV circular dichroism spectra of thioredoxin (49 μM protein). In panels A−C, the dashed lines represent spectra obtained at pH 7 (in 30 mM sodium phosphate buffer) and the solid lines represent spectra obtained at pH 3 (in 30 mM glycine buffer). (D) Equilibrium unfolding curves of thioredoxin at pH 7 (○) and 3 (△), determined by measurement of ellipticity at 222 nm. The equilibrium unfolding curves were converted to plots of fraction of protein unfolded vs GdnHCl concentration and fitted to a two-state N ⇌ U model for unfolding, as described in ref *48*. The solid line through the data represents the fit, which yielded values for ΔG, the free energy of unfolding, and C_m, the midpoint of the transition, of 8.2 kcal/mol and 2.5 M, respectively.

Native Trx Has 33 Amide Hydrogen Sites Protected from HX at pH 3. Figure 2A shows exchange-out of amide deuteriums from deuterated Trx at pH 3. In the inset of Figure 2A, exchange-out is seen to manifest itself in a shift in the mass spectrum to lower *m*/*z* values with the time of exchange-out. Only one peak with a decreasing average mass and width with time is observed, suggesting that the exchange mechanism is EX2 (*9*, *32*). The number of protected amide deuteriums at each time of incubation was determined by subtracting the mass of the protonated protein (11 673 Da) from the mass observed at that time. Fully deuterated Trx has a mass 180 Da greater than that of protonated Trx, indicating that 180 protons are replaced with deuteriums. Figure 2A shows that at the earliest time (3 min) of incubation of the deuterated protein in H_2O, the number of deuteriums retained has been reduced to 90, indicating that 90 deuteriums have exchanged out very rapidly. The number of deuteriums retained decreases with time, and after 20−24 h, exchange-out appears to have reached a plateau level, where 33 ± 3 deuterons are retained in each Trx molecule. Thus, Trx has 33 ± 3 amide hydrogen sites that are protected from exchange at pH 3. When exchange-out of amide deuteriums from Trx is carried out at pH 7 (Figure 2B), where the intrinsic HX rate is 10^4 times faster than it is at pH 3, 13 of these 33 amide hydrogen sites exchange out over a 3 h time period, and the protein is seen to have 20 ± 3 amide hydrogen sites that are protected from exchange at pH 7. These results are in accordance with previous studies which had shown that 27 amide hydrogen sites remain protected from exchange at pH 5.7 (*47*). The results in panels

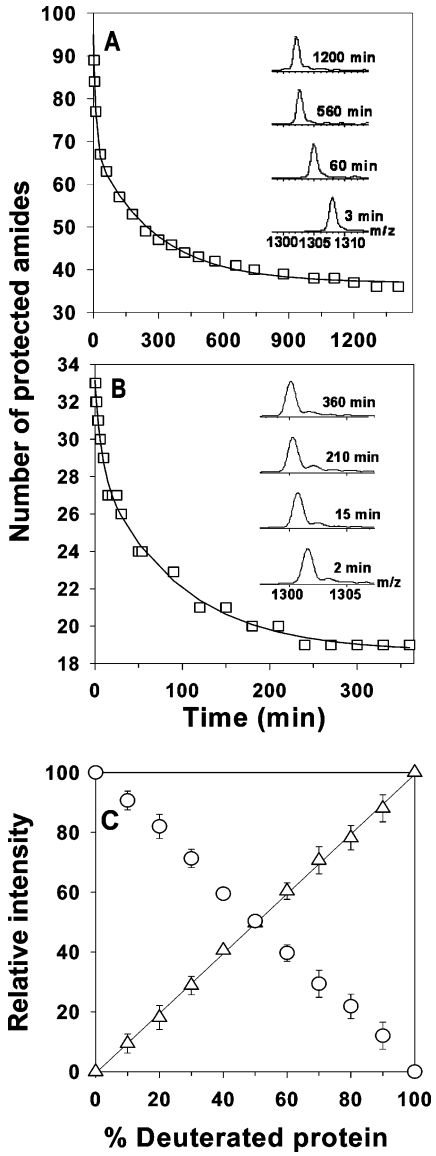

FIGURE 2: Kinetics of deuterium−proton exchange from native thioredoxin. A solution of deuterated Trx in D_2O was diluted 50-fold into H_2O buffer (50 mM glycine) at pH 3 (A) or 10-fold into H_2O buffer (50 mM sodium phosphate) at pH 7 (B). Panel A shows how the number of protected amide deuterium atoms, N_D, decreases with time of incubation in H_2O at pH 3. The solid line through the data is described by the equation $N_D = 36 + 27 \times \exp(-0.089t) + 32 \times \exp(-0.0035t)$. The inset shows the mass spectra (the ninth charged state) of the protein at different times of incubation in H_2O. Panel B shows how the number of protected amide deuterium atoms decreases with time of incubation in H_2O at pH 7. The solid line through the data is described by the equation $N_D = 19 + 4 \times \exp(-0.135t) + 10 \times \exp(-0.01t)$. The inset shows the mass spectra (the ninth charged state) of the protein at different times of incubation in H_2O. Panel C shows that the relative populations of deuterated and fully protonated Trx molecules in a mixture of the two, determined from the relative ion intensities of the ninth charged states centered at *m*/*z* 1301.8 (deuterated Trx, with 32 protected deuteriums) and *m*/*z* 1298.6 (protonated Trx), scale linearly with the molar ratio at which the deuterated and protonated molecules were mixed.

A and B of Figure 2 also indicate that the native protein has at least five classes of amide hydrogen sites that differ in their level of protection. From the measured rate of exchange-out at each class of amide hydrogen site (Figure 2 legend), and assuming an intrinsic HX rate of 20 s^{-1} at pH 7 and of

0.002 s^{-1} at pH 3 at 25 °C (*51*), the protection factors of the five classes are calculated to be, approximately, 1.5, 35, 9000, 120000, and >120000.

Determination of the Relative Amounts of Deuterated and Protonated Trx in a Mixture. For proper analysis of HX-MS measurements of protein folding, it is important to first show that the fully protonated protein population and the deuterated (33 ± 3 deuteriums) protein population can be estimated quantitatively in a mixture of the two populations, from the relative ion intensities of the two peaks that are observed for the ninth charged states of the two forms. Figure 2C shows that this is indeed so: when deuterated and protonated protein are mixed at different molar ratios in H_2O at pH 3, the relative ion intensities of the two peaks corresponding to the two forms differing in mass by 33 Da predict the molar ratios of mixing. This experiment also indicates that there is no significant exchange-out from the samples within the mass spectrometer. Thus, if both N and U molecules are present together, they can be distinguished by the former but not the latter possessing 33 amide hydrogen sites that are protected from exchange.

Unfolding of Trx at pH 7 Monitored by HX-MS and by Optical Probes. HX-MS was used to determine the fraction of protein that is unfolded, at each of three different GdnHCl concentrations corresponding to the transition zone of the equilibrium unfolding curve. This unique capability of HX-MS arises because 33 amide hydrogen sites are stable to HX in the N state but undergo exchange in the U form. Hence, the result of proton labeling of a mixture of native and unfolded protein that had been previously deuterated is that the native protein retains deuterium at 33 amide hydrogen sites while unfolded protein does not; consequently, the unfolded protein will have a mass that is 33 Da lower than that of the native protein. Figure 3A shows that the fraction of protein that is unfolded at each GdnHCl concentration agrees well with the value estimated from the fluorescence, far-UV CD, or near-UV CD-monitored equilibrium unfolding curves. The mass spectrum obtained from each of the protein samples, equilibrated at any of the three GdnHCl concentrations, shows only two well-resolved peaks, corresponding to deuterated (11 706 Da) and protonated (11 673 Da) protein and originating from the native and unfolded protein populations present at equilibrium (inset in Figure 3A). The absence of any ion intensity straddling the two peaks indicates the absence of any intermediate showing protection at only a subset of the 33 most protected amide hydrogen sites. It should be noted that because the labeling pulse had a duration of 5 s and because the intrinsic time constant of HX at pH 7 and 25 °C is 50 ms, any intermediate with a protection factor of ≤20 at each of the 33 amide hydrogen sites stable to HX could also have become fully labeled and appeared as U. Such a possibility appears unlikely because the relative amount of U determined by HX-MS is predicted by the optically monitored equilibrium unfolding curves.

Figure 3B shows how the amount of unfolded protein increases with time of unfolding in 3 M GdnHCl. The mass spectra show only two well-resolved peaks at each time of unfolding (inset in Figure 3B), indicating that U and N are the only two forms present at any time during the unfolding reaction. Figure 3B shows that the fraction of protein unfolded shows an exponential dependence on the time of unfolding, with an apparent rate of 0.008 s^{-1}, and indicates that there is virtually no (<10%) U present at the earliest time of unfolding that was monitored. Thus, the unfolding kinetics also indicate that N unfolds directly to U, although it is possible that an intermediate with weak general protection against HX (see above) may be transiently populated.

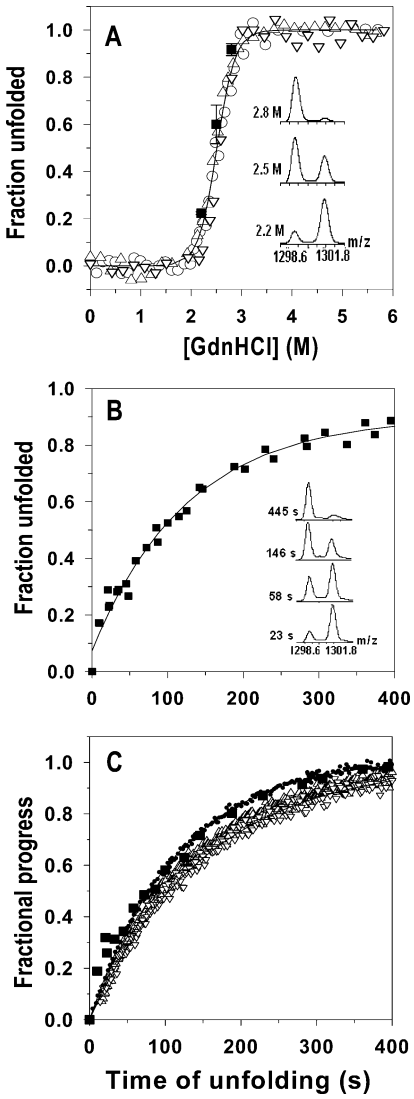

FIGURE 3: Equilibrium and kinetic unfolding studies of thioredoxin at pH 7. Unfolding was monitored by HX-MS (■), as well as by fluorescence (○), ellipticity at 222 nm (△), and near-UV CD (▽). Panel A shows the values of the fraction of protein that is unfolded, which were determined by HX-MS at three GdnHCl concentrations, overlaid on the values of fractional changes in the magnitude of the optical signal, which were determined from equilibrium unfolding curves. The inset shows the mass spectra of samples unfolded in 2.2, 2.5, and 2.8 M GdnHCl. Panel B shows how the relative amount of unfolded protein (■), determined by HX-MS, increases with time of unfolding in 3 M GdnHCl. The solid line through the data represents a single-exponential fit to the data and yields an apparent constant of unfolding of 0.008 s^{-1}. Representative mass spectra of samples in which the labeling pulse was given at the indicated times are shown in the inset. Panel C compares the kinetics of unfolding in 3 M GdnHCl monitored by HX-MS to the kinetics monitored by the three optical probes. The kinetic curves were normalized between a value of 0 for the native protein at time zero and a value of 1 at the end of the kinetic curve ($t = \infty$). The solid line is a single-exponential fit to the data and yields a value for the observed rate of unfolding, λ, of 0.0085 s^{-1}.

Figure 3C compares the kinetics of unfolding of Trx, measured by near-UV CD, far-UV CD, and fluorescence, to the kinetics of unfolding measured by HX-MS. For each probe, a single kinetic phase accounts for the complete amplitude of unfolding. The probes for tertiary structure, near-UV CD, and fluorescence and the probe for secondary structure, far-UV CD all yield very similar kinetics. An earlier study (*46*) had shown co-incident kinetics for unfolding in 3.2 M GdnHCl, when monitored by fluorescence and far-UV CD. The observation suggests that unfolding at pH 7 can be described by a two-state N ⇌ U model. Not surprisingly then, the increase in the relative amount of unfolded protein, as measured by HX-MS, occurs at a rate identical to the rate measured by the fractional changes in the optical signals (Figure 3C).

Unfolding of Trx at pH 3 Monitored by HX-MS and by Optical Probes. Figure 4A shows that an equilibrium GdnHCl-induced unfolding curve determined by monitoring the change in far-UV CD is co-incident with that determined by monitoring the change in fluorescence. Both unfolding curves have a midpoint (C_m) at 2.5 M. In contrast, the equilibrium unfolding curve determined by monitoring the change in near-UV CD does not overlap with the other two and has a different value for C_m at 2.26 M GdnHCl. The fraction of protein that remains folded at pH 3, at each of the different GdnHCl concentrations corresponding to the transition zone of the equilibrium unfolding curve, was determined using HX-MS. This fraction is found to be predicted by the fractional retention of near-UV CD at each GdnHCl concentration. Together, the optical and HX-MS studies suggest that equilibrium unfolding at pH 3 is described minimally by a three-state N ⇌ I_E ⇌ U model, where I_E is a partially folded intermediate which has lost the near-UV CD signal of native Trx.

The mass spectrum obtained from each of the protein samples, equilibrated at any of the three GdnHCl concentrations, showed two peaks, corresponding to deuterated (11 706 Da) and protonated (11 673 Da) protein, and originating from the native and unfolded protein populations present at equilibrium (inset in Figure 4A). But unlike in the case of the samples equilibrated at pH 7 (Figure 3A), the peaks are not well resolved: 12−20% of the total ion intensity spans the region between the two peaks. This result suggests that the intermediate I_E represents one or more intermediates that afford significant protection to one or more subsets of the 33 amide hydrogen sites most protected from exchange in native Trx. In an earlier study (*39*), equilibrium intermediates were reported to be populated during equilibrium thermal denaturation at low pH.

Figure 4B shows how the amount of unfolded protein increases with time of unfolding in 3 M GdnHCl. The mass spectra show two peaks at each time of unfolding (inset in Figure 4B) corresponding to the U and N forms. There also appears to be some amount (10−15%) of ion intensity that spans the region between the two peaks, for the mass spectrum after unfolding for 10 s, suggesting that N and U are not the only two forms present at early times of unfolding. Figure 4B shows that the fraction of protein unfolded shows an exponential dependence on the time of unfolding, with a rate of 0.01 s^{-1}. The kinetic curve for unfolding does not, however, extrapolate to zero U at zero time of unfolding, as it appears to for unfolding at pH 7 (Figure 3B), but instead

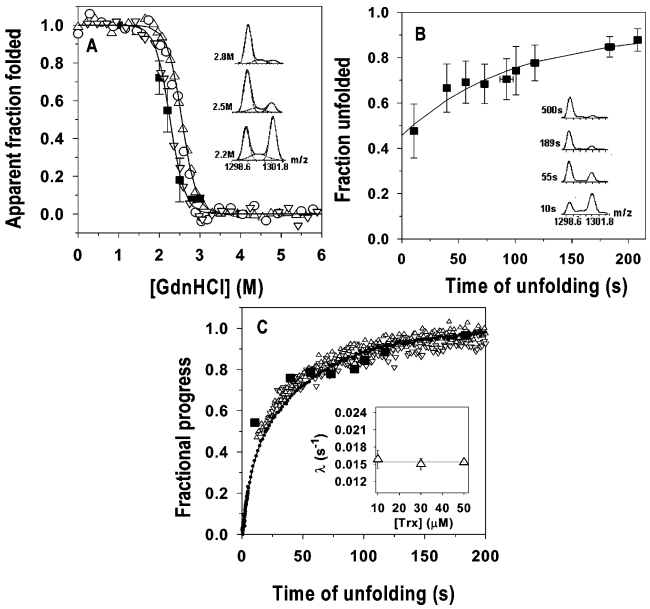

FIGURE 4: Equilibrium and kinetic unfolding studies of thioredoxin at pH 3. Unfolding was monitored by HX-MS (■), as well as by fluorescence (○), ellipticity at 222 nm (△), and near-UV CD (▽). Panel A shows the values of the fraction of protein that remains native, which was determined at different GdnHCl concentrations by HX-MS, overlaid on the values of the fractional changes in the magnitude of the optical signal, which were determined from equilibrium unfolding curves. The inset shows the mass spectra (ninth charged state) of samples labeled in 2.2, 2.5, and 2.8 M GdnHCl. The mass spectra were fit to the sum of three Gaussian distributions, shown as dotted lines. The fraction of native protein at each GdnHCl concentration was determined from the relative area under the Gaussian distribution corresponding to the peak of the deuterated protein (at *m*/*z* 1301.8); all native protein remains deuterated even after the labeling pulse. The fractions of protein molecules present as an intermediate (with protection and, hence, labeled mass intermediate between that of U and N) at different GdnHCl concentrations were estimated to be 0.12 (2 M), 0.21 (2.2 M), 0.18 (2.5 M), and 0.13 (2.8 M). Panel B shows how the relative amount of unfolded protein (■), determined by HX-MS, increases with time of unfolding in 3 M GdnHCl. The solid line through the data represents a single-exponential fit to the data and yields an apparent rate constant of unfolding of 0.01 s^{-1}. The inset shows representative mass spectra (ninth charged state) of samples in which the labeling pulse was applied at the indicated times. Panel C compares the kinetics of unfolding in 3 M GdnHCl monitored by HX-MS to the kinetics monitored by the three optical probes. The kinetic curves were normalized between a value of 0 for the native protein at time zero and a value of 1 at the end of the kinetic curve ($t = \infty$). The solid line is a fit of the fluorescence-monitored data to a two-exponential equation and is described by the equation $F(t) = 0.35 \times \exp(-0.12t) + 0.65 \times \exp(-0.017t)$. The inset shows how the slow observed rate constant, λ, of unfolding in 3 M GdnHCl, which was monitored by measurement of ellipticity at 222 nm (△), varies with protein concentration in the range of 5−50 μM. The error bars represent standard deviations of measurements from three separate experiments.

indicates that ∼45% of the molecules have formed U, or a species that affords U-like protection from HX (with a protection factor of ≤20) at all 33 protected amide hydrogen sites, at the earliest time (11 s) of unfolding monitored. The observation that only 90% of the molecules have unfolded even after 500 s (Figure 4B) is expected because the equilibrium unfolding studies (Figure 4A) indicate that 10% of the molecules remain as N (or I_E) in 3 M GdnHCl at pH 3.

Figure 4C compares the kinetics of unfolding of Trx in 3 M GdnHCl, measured by near-UV CD, far-UV CD, and

fluorescence, to the kinetics of unfolding measured by HX-MS. Since the fluorescence-monitored kinetics were measured by rapid mixing in a stopped-flow machine, the entire amplitude of the unfolding reaction could be observed. The change in fluorescence occurs in two kinetic phases, a fast phase accounting for 35% of the amplitude and a slow phase accounting for 65% of the amplitude. Far-UV CD-monitored and near-UV CD-monitored kinetics were measured only in manual mixing experiments, whose time resolution is sufficient to capture only the slow phase seen in the fluorescence-monitored kinetics. It is observed that the kinetic curves for the slow changes in far-UV CD and near-UV CD coincide with the kinetic curve observed for the slow change in fluorescence (Figure 4C). The kinetics of the increase in the fraction of protein unfolded, as determined by a manual mixing HX-MS experiment, also appear co-incident with the kinetics of the slow phase monitored by the three optical probes. The observation that unfolding in 3 M GdnHCl at pH 3 occurs in two kinetic phases indicates that unfolding at pH 3 cannot be described by a two-state N $\rightleftharpoons$ U model but that at least one additional species must be incorporated into any unfolding model. The HX-MS results also indicate that in the fast phase of unfolding, 45% of the protein molecules have unfolded either to U or to an intermediate with a protection factor of $\leq$20 at each of the 33 amide hydrogen sites stable to HX (see above).

Since the concentration of Trx used in the unfolding experiments spanned the range of 5−50 μM, depending on the probe being used, it was important to demonstrate that the unfolding kinetics were independent of protein concentration in this range. The inset in Figure 4C shows that the unfolding rates in 3 M GdnHCl at pH 3, as measured by the change in ellipticity at 222 nm, do not vary with protein concentration in this range.

Dependence on GdnHCl Concentration of the Unfolding Kinetics at pH 3. Panels A and B of Figure 5 compare the kinetics of unfolding, determined by measurement of fluorescence, far-UV CD, and near-UV CD, at pH 3, in 2.2 and 2.5 M GdnHCl, respectively. At these denaturant concentrations, the equilibrium intermediate appears to be populated maximally (Figure 4A), and the midpoint of the near-UV CD-determined equilibrium unfolding curve is at 2.26 M GdnHCl. For unfolding in 2.2 M GdnHCl, the far-UV CD-monitored kinetic trace extrapolates to approximately the value expected for the native protein at time zero, while the near-UV CD-monitored kinetic trace extrapolates to a significantly non-zero value. This suggests that the transient accumulation of an initial intermediate, I_1, within 10 s, which has lost ~40% of the near-UV ellipticity characteristic of native protein but practically none of the far-UV CD. Unexpectedly, the fluorescence-monitored kinetic trace while commencing at the value expected for the native protein shows an initial dip and then rise, suggesting the population of a late intermediate after unfolding for ~50 s. This late intermediate, I_2, possesses less fluorescence intensity than native protein and appears to subsequently unfold to I_E and U which are together present at equilibrium in 2.2 M GdnHCl at pH 3 (Figure 4A).

For unfolding in 2.5 M GdnHCl, the fluorescence-monitored and far-UV CD-monitored kinetic traces extrapolate within experimental error to the values expected for the native protein at time zero, while the near-UV CD-monitored kinetic trace does not. These results indicate that for unfolding in 2.5 M GdnHCl, too, an intermediate species I_1, which has lost some of the near-UV CD signal characteristic of the native protein but none of the fluorescence or far-UV CD signal, is populated within a few seconds of unfolding. Intermediate I_2, which can be detected easily during unfolding in 2.2 M GdnHCl, appears not to be populated to any significant extent during unfolding in 2.5 M GdnHCl.

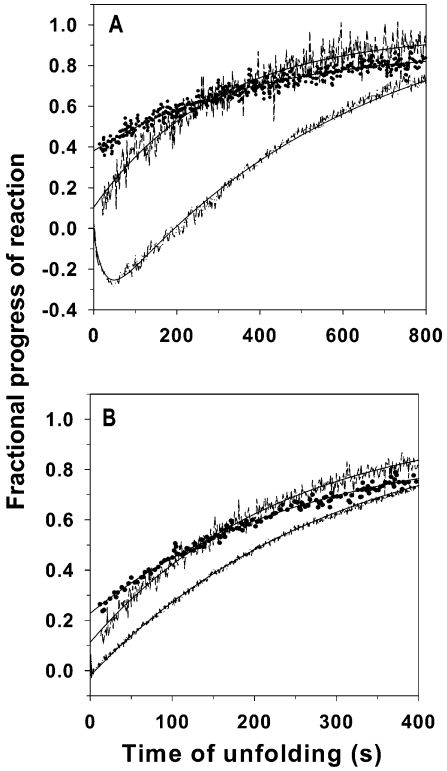

FIGURE 5: Optically monitored kinetics of unfolding of Trx at pH 3. Unfolding in 2.2 M GdnHCl (A) and in 2.5 M GdnHCl (B) was monitored by fluorescence (−••−), far-UV CD (− − −), and near-UV CD (•••). For each kinetic trace, the fractional progress of the reaction was calculated as $(S_t - S_0)/(S_\infty - S_0)$, where S_t is the value of the signal at time t of unfolding, S_0 is the value of the signal corresponding to that of the native protein, and S_∞ is the value of the signal at infinite time. For each trace, only the first 800 s (A) or the first 500 s of the kinetic traces acquired is shown, but the traces were acquired for at least 3τ s, where τ is the observed time constant. The solid line through the CD-monitored kinetic trace is a nonlinear least-squares fit to a single-exponential process; for the fluorescence-monitored kinetic trace in panel A, the fit was carried out to the sum of a two-exponential equation. The fits yielded values for the observed slow rates of unfolding, when determined by fluorescence, far-UV CD, and near-UV CD, of 0.0017, 0.0034, and 0.0026 s^{-1} in 2.2 M GdnHCl and of 0.0033, 0.0043, and 0.0039 s^{-1} in 2.5 M GdnHCl, respectively.

Since the fraction of molecules unfolding at these low concentrations of GdnHCl is less than 20%, it was not possible to determine the kinetic trace of unfolding by HX-MS, which was possible at 3 M GdnHCl (Figure 4B).

Figure 6 shows how the unfolding kinetics at pH 3 vary with GdnHCl concentration. In Figure 6A, it is seen that the observed rate of slow unfolding at any GdnHCl concentration is the same, regardless of the probe used to assess unfolding. The dependences on GdnHCl concentration of the logarithm of fast and slow observed rate constants are also seen to be almost identical.

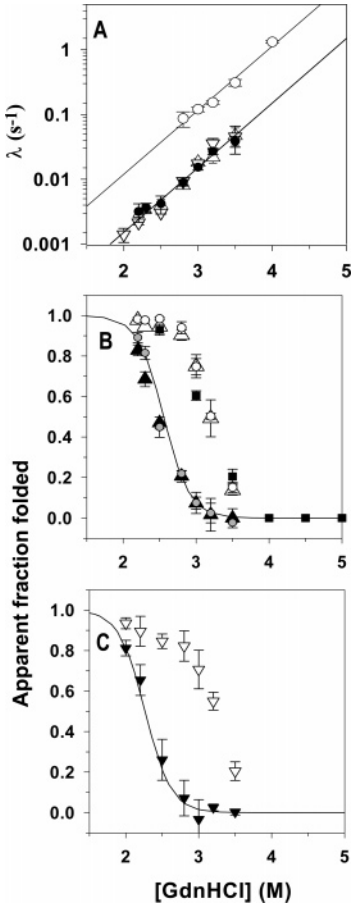

FIGURE 6: GdnHCl concentration dependence of unfolding kinetics at pH 3. Unfolding in different denaturant concentrations was monitored by HX-MS (■), far-UV CD (△ and ▲), near-UV CD (▽ and ▼), and fluorescence (○ and ●). Panel A shows how the observed rate constants of unfolding depend on GdnHCl concentration. The straight line fitted through the observed fast rate constants (λ^f) of unfolding is described by the equation $\log \lambda^f = -3.9 + 0.98$[GdnHCl], and the straight line fitted through the observed slow rate constants (λ^s) of unfolding is described by the equation $\log \lambda^s = -4.81 + 0.99$[GdnHCl]. Panel B compares the kinetic amplitude of the slow phase of unfolding to the equilibrium amplitude of unfolding, when unfolding is monitored by measuring changes in far-UV CD or fluorescence. The solid line represents the fit to the fluorescence and far-UV CD-monitored equilibrium unfolding curve shown in Figure 4A. White symbols represent the $t = 0$ point of the slow kinetic phase of unfolding, and black symbols represent the $t = \infty$ point of the unfolding reaction. The fractions of protein molecules that have remained folded after unfolding for 11 s at different concentrations of unfolding buffer, which were determined from HX-MS experiments, are also shown. Panel C compares the kinetic amplitude of the slow phase of unfolding to the equilibrium amplitude of unfolding, when unfolding is monitored by measuring the change in near-UV CD. The solid line represents the fit to the near-UV CD-monitored equilibrium unfolding curve shown in Figure 4A. In all panels, the error bars represent standard deviations of measurements from three separate experiments.

Figure 6B compares the kinetic and equilibrium amplitudes for unfolding monitored by fluorescence as well as by far-UV CD. For both fluorescence- and far-UV CD-monitored kinetic unfolding studies, the $t = \infty$ points of the kinetic unfolding traces fall on the equilibrium unfolding transition determined by the fluorescence or far-UV CD measurements, as expected. The $t = 0$ points of the slow phase of kinetic unfolding traces monitored by the two probes fall on each other, and they exhibit a sigmoidal dependence on the concentration of GdnHCl in which unfolding was carried out. This sigmoidal dependence, characterized by a C_m value of 3.2 M GdnHCl, represents the unfolding transition of the species that is populated at the end of the fast phase of unfolding at pH 3.

Figure 6C compares the kinetic and equilibrium amplitudes for unfolding monitored by near-UV CD. Again, the $t = \infty$ points of the kinetic unfolding traces fall on the equilibrium unfolding transition determined by near-UV CD measurements, as expected. As already evident from Figure 5, the $t = 0$ points of the kinetic unfolding traces for unfolding at GdnHCl concentrations in the range of 2−2.8 M (Figure 6C) do not overlap with the $t = 0$ points of the corresponding kinetic traces obtained using far-UV CD or fluorescence (Figure 6B). For unfolding in this range of GdnHCl concentrations, the fractional change in near-UV CD in the fast phase of unfolding is seen to be 10−30% more than the corresponding fractional change in far-UV CD or fluorescence (Figure 5). The $t = 0$ points of the kinetic traces monitored by near-UV CD show a sigmoidal dependence on the concentration of GdnHCl in which unfolding was carried out, which is significantly broader than that seen when unfolding is monitored by fluorescence or far-UV CD. This broad sigmoidal dependence is characterized by a C_m value of 3.1 M.

To determine the fraction of molecules that remain as N (or an intermediate equally stable to HX) before the slow phase of unfolding has proceeded to any significant extent, 5 s HX labeling pulses were applied at 11 s of unfolding at different GdnHCl concentrations in the range of 2.5−5 M. Figure 6B shows that the fraction of molecules not labeled at all (and, hence, present as N or an intermediate as stable as N) at this time of unfolding decreases with an increase in the concentration of GdnHCl present during unfolding, in a manner similar to the decrease seen in the fractional amplitude of the slow change in fluorescence or far-UV CD. This result indicates that initial intermediate I_1, which has partially lost near-UV ellipticity (Figure 5A), confers as much protection as N at each of the 33 amide sites that are stable in N.

Dependence of Unfolding Kinetics at pH 3 on Protein Concentration. Although the observed slow rate constant of unfolding in 3 M GdnHCl at pH 3 does not vary when the protein concentration is varied in the range of 5−50 μM (Figure 4C, inset), it is significantly lower when the unfolding reaction is carried out at much higher protein concentrations. The deceleration of the slow unfolding reaction at high protein concentrations can be observed when unfolding is monitored by HX-MS. Figure 7A shows that the observed slow rate of unfolding at a protein concentration of 850 μM is significantly slower than that measured at a protein concentration of 50 μM (Figure 4B). Figure 7B compares the near-UV CD-monitored kinetic trace of unfolding in 3 M GdnHCl of 50 μM Trx to that of 200 and 500 μM Trx, and Figure 7C does likewise for unfolding in 2.2 M GdnHCl. When Trx is unfolded at a concentration of 500 μM in 2.2 M GdnHCl at pH 3, the relative loss of near-UV ellipticity is also much smaller than at a concentration of 50 μM. Figure 7D shows how the observed slow rate constant of unfolding in 3 M GdnHCl at pH 3 decreases with an increase in protein concentration. In contrast, when the unfolding of Trx in 3

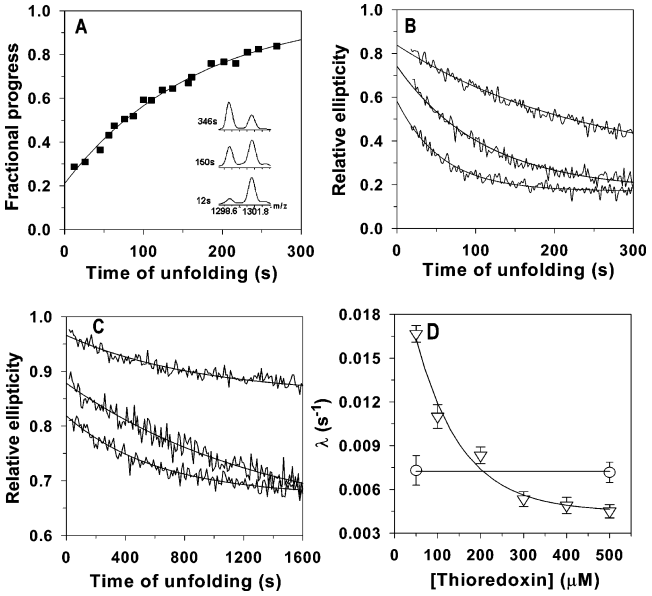

FIGURE 7: Kinetics of unfolding of Trx at high protein concentrations and pH 3. Panel A shows how the fraction of unfolded protein increases with time of unfolding of 850 μM Trx in 3 M GdnHCl, as determined by HX-MS (■). The inset shows representative mass spectra obtained at different times of unfolding. The kinetic trace in panel A was normalized between a value of 0 for the native protein at time zero and a value of 1 for infinite time. The solid line through the data is a single-exponential fit, which yields a value for the observed rate constant, λ_U, of slow unfolding of 0.006 s^{-1}. Panel B shows the kinetics of unfolding in 3 M GdnHCl of Trx at 50 (bottom trace), 200 (middle trace), and 500 μM (top trace), when monitored by measurement of ellipticity at 270 nm. The kinetic traces were fit to single-exponential equations; the fits are shown as solid lines through the data. The observed rates of unfolding were 0.017 s^{-1} at 50 μM, 0.009 s^{-1} at 200 μM, and 0.004 s^{-1} at 500 μM. Panel C shows the kinetics of unfolding in 2.2 M GdnHCl of Trx at 50 (bottom trace), 200 (middle trace), and 500 μM (top trace), when monitored by measurement of ellipticity at 270 nm. Each kinetic trace was fit to a single-exponential equation; the fits are shown as solid lines through the data. The observed rates of unfolding were 0.0016 s^{-1} at 50 μM, 0.0007 s^{-1} at 200 μM, and 0.001 s^{-1} at 500 μM. In panels B and C, each kinetic trace is normalized relative to a value of 1 for the signal of the native protein at the relevant protein concentration. Panel D shows the dependence of the near-UV CD-monitored, observed slow rates of unfolding in 3 M GdnHCl at pH 3 (▽) on Trx concentration in the range of 50−500 μM. For comparison, the values of the near-UV CD-monitored, observed rates of unfolding in 3 M GdnHCl at pH 7 (○) for 50 and 500 μM Trx are also shown. The solid lines through the data in panel C have been drawn by inspection only. The error bars represent the standard deviations of the measurements from three separate experiments.

M GdnHCl was monitored by near-UV CD at pH 7, the observed unfolding rate constant that was determined was found to be the same for unfolding at concentrations of 50 and 500 μM.

DISCUSSION

The unfolding of Trx at pH 7 appears to be simple and occur in one step, with different probes yielding very similar unfolding kinetics (Figure 3). On the other hand, unfolding at pH 3 appears to be complex and to occur in several steps, with different probes yielding different kinetics (Figures 4−6). Before considering a possible mechanism for unfolding at pH 3, it is necessary to consider the coupling of proline isomerization reactions to the actual unfolding step, because it is well-known that such coupling complicates the analysis of even simple unfolding reactions (*52*). Consideration of cis to trans proline isomerization is particularly important in the case of Trx, for the unfolded as well as native states, because it has one proline residue, Pro76, which exists in the cis conformation in the native state (*37*).

Coupling of the Unfolding Reaction to Proline Isomerization. Native Trx has been characterized extensively by NMR (*47*, *53*−*55*) as well as by MS (*38*−*41*). These studies have not provided any evidence of multiple native states resulting from cis−trans proline isomerization in the native protein, as they have for other proteins (*6*, *56*−*59*). Hence, it is very unlikely that the unfolding kinetics of Trx are complex at pH 3 because of the presence of two native states in slow equilibrium with each other. The cause of the complexity must lie in processes that occur during unfolding.

In fact, previous studies had in fact shown that the unique native state, N, unfolds by a $N \rightleftharpoons U_C \rightleftharpoons U_T$ mechanism (*45*, *46*), in which the unfolding reaction is followed by and coupled to proline isomerization reactions in the unfolded state (*42*−*46*). The unfolded state having Pro76 in a cis conformation (U_C) is formed initially and equilibrates with other unfolded forms having Pro76 in the trans form (U_T), with a relaxation rate of ∼0.02−0.03 s^{-1}, which is independent of the concentration of the denaturant.

For a protein such as Trx, which has one cis proline residue in the native state, the observed unfolding kinetics will depend on the concentration of denaturant and on whether the unfolding reaction is faster or slower than the subsequent proline isomerization reaction (*52*). When the $N \rightleftharpoons U_C$ reaction is slower than the $U_C \rightleftharpoons U_T$ reaction, unfolding is expected to occur in a single kinetic phase, for concentrations of GdnHCl larger than or equal to the concentrations corresponding to the equilibrium unfolding transition zone (*52*). This appears to be the case at pH 7, where unfolding occurs in a single kinetic phase with the same rate measured by different probes (Figure 3).

At pH 3, unfolding occurs in two kinetic phases (Figure 6). The fast phase has a rate that is 10-fold faster than that of the unfolding phase at pH 7. It therefore appears that the unfolding reaction at pH 3 is faster than the subsequent proline isomerization reaction. When this is the case, unfolding is expected to occur in two kinetic phases for concentrations of GdnHCl larger than or equal to the concentrations corresponding to the equilibrium unfolding transition zone, even when all optical signals used to monitor the unfolding change only during the faster $N \rightleftharpoons U_C$ step (*52*). The relative amplitude of the faster phase is expected to grow at the expense of that of the slower phase, with an increase in GdnHCl concentration, and the rates of both kinetic phases are expected to exhibit somewhat similar exponential dependences on GdnHCl concentration for GdnHCl concentrations corresponding to those in the equilibrium unfolding transition zone. Both expectations are met (Figure 6). Hence, at pH 3, the fast observed rate constant represents the $N \rightleftharpoons U_C$ reaction, while the slow observed rate constant is that of the subsequent proline isomerization reaction (*52*).

It is possible to verify that the $N \rightleftharpoons U_C \rightleftharpoons U_T$ mechanism is appropriate for describing the biphasic unfolding kinetics at pH 3 (Figure 4). At equilibrium, 10% of the unfolded molecules are known to exist as U_C (*46*). Thus, U_C is

expected to be ~1.4 kcal/mol more unstable than the equilibrium unfolded protein (*47*). The data in Figure 6B indicate that this is indeed so. The unfolding transition traced by the $t = 0$ points of the slow fluorescence and far-UV CD kinetic traces, which represents the unfolding of N to U_C, has a midpoint at 3.1 M, while the equilibrium unfolding transition determined by the same optical probes has a midpoint at 2.5 M. Since both unfolding transitions have the same slope ($m = 3.2$ kcal mol^{-1} M^{-1}), the data in Figure 6B indicate that U_C is ~1.8 kcal/mol more unstable than the equilibrium unfolded protein. Moreover, the mechanism demands that the product of the fast phase of unfolding be primarily unfolded protein, and the HX-MS studies indicate that this is indeed so at all GdnHCl concentrations in the range of 2.5−5 M (Figure 6B). Only a fraction of the protein molecules unfold completely in the fast phase to U_C. In the slow phase of unfolding, U_C equilibrates with U_T, and as a result of the coupling between the unfolding and proline isomerization reactions, the remaining N molecules unfold at a rate limited by that of the proline isomerization reaction. Hence, the $N \rightleftharpoons U_C \rightleftharpoons U_T$ mechanism is the simplest possible mechanism that can explain all the data.

Unfolding at pH 7 Can Be Described by a Two-State $N \rightleftharpoons U$ Model. No partially unfolded intermediate can be detected at pH 7, when unfolding studies are carried out at equilibrium. All three optical probes, fluorescence, far-UV CD, and near-UV CD, yield the same equilibrium unfolding curve, suggesting that N and U are the only forms populated at all concentrations of GdnHCl. In this study, it has been shown that HX-MS, unlike the optical probes, can distinguish between, as well as quantitatively estimate, the populations of native and unfolded Trx molecules when both coexist, as they do in the unfolding transition zone of an equilibrium unfolding curve. The observation that the fraction of protein which is unfolded, determined by HX-MS, can be predicted by the fractional change in either of the three spectroscopic probes, at different concentrations of GdnHCl that define the transition zone of equilibrium unfolding, constitutes strong evidence for the two-state nature of the unfolding of Trx at pH 7.

Similarly, no intermediate is detected in kinetic studies. At different concentrations of GdnHCl, unfolding is described by a single-exponential process that accounts for the complete amplitude of the spectroscopic change that accompanies the unfolding reaction. The fractional change in optical signal at any time of unfolding predicts the fraction of protein that has become unfolded at that time. Thus, in both equilibrium and kinetic experiments, the unfolding of Trx at pH 7 appears to be adequately described by a two-state $N \rightleftharpoons U$ model.

Unfolding at pH 3 Cannot Be Described by a Two-State $N \rightleftharpoons U$ Model. In equilibrium studies of the unfolding of Trx at pH 3, the observation that the equilibrium unfolding curve determined by monitoring the change in the near-UV CD signal does not coincide with that determined by monitoring the change in fluorescence or far-UV CD indicates that at least one intermediate, I_E, is populated in equilibrium with N and U. In HX-MS studies, I_E manifests itself as a species with a U-like lack of stability to exchange in at least a subset of the 33 amide hydrogens that are stable to exchange in N. Given that the extent of protection in I_E straddles that seen in U and N, it is likely that I_E resembles an ensemble of structures, in each of which a different subset of amide hydrogens have lost their stability to exchange. Since the fractional decrease in the population of native molecules with an increase in GdnHCl concentration in the equilibrium unfolding studies is given by the fractional decrease in the magnitude of the near-UV CD signal, a spectroscopic signature of I_E is the fact that it is devoid of a near-UV signal.

If the unfolding at pH 3 occurs by a simple three-state $N \rightleftharpoons U_C \rightleftharpoons U_T$ mechanism, then the kinetics of the fast and slow phases are expected to be the same whether measured by fluorescence, far-UV CD, or near-UV CD, as long as U_C and U_T have identical optical properties as expected for completely unfolded forms. If either the relative amplitude or the unfolding rate of either kinetic phase is found to be probe-dependent, it would suggest the presence of one or more intermediates on the unfolding pathway between N and U_C. The data in Figures 5 and 6 indicate that when unfolding is carried out at concentrations of denaturant in the range of 2.2−2.5 M, the relative amplitude of the fast (subsecond) phase of change in the near-UV CD signal is 10−30% more than that of the fast phases of changes in far-UV CD and fluorescence signals. As a result, the curve traced by the $t = 0$ points of the near-UV CD-monitored kinetic traces of unfolding does not overlap the corresponding curves determined from far-UV CD or fluorescence-monitored kinetic experiments. If the species present at the end of the fast phase were only the unfolded form, U_C, as expected from the $N \rightleftharpoons U_C \rightleftharpoons U_T$ mechanism, then all three optical probes should have given the same relative amplitude of signal change accompanying the subsecond phase of unfolding, and hence, all three curves traced by the $t = 0$ points should have been overlapping. The results therefore indicate that in addition to U_C, one or more intermediates that have lost some of the native-state near-UV CD signal but not the far-UV CD or fluorescence signal are also populated before the start of the slow phase of unfolding.

The equilibrium intermediate at pH 3 has not only lost protection against HX at a subset of the 33 most stable amide hydrogen sites but also lost its near-UV CD signal. Since an intermediate can be detected in kinetic studies by virtue of it having lost near-UV CD, this intermediate might also be expected to have lost protection (at least partially) against HX, in a manner similar to that observed in the equilibrium intermediate. But it appears that the kinetic intermediate that is populated initially during unfolding in 2.2−2.5 M GdnHCl has not lost protection against HX (Figure 6). It therefore appears that for unfolding in this range of GdnHCl concentrations, near-UV ellipticity is first lost, and then further unfolding occurs leading to a partial loss of protection against HX.

In fact, the data in Figure 5A do suggest that unfolding in 2.2 M GdnHCl at pH 3 occurs in multiple steps. Near-UV ellipticity is lost in less than 10 s, corresponding to formation of intermediate I_1, and then over a 50 s time domain, intermediate I_2 with a tryptophan fluorescence lower than that of N is formed. Finally, at equilibrium, intermediate I_E which has U-like near-UV ellipticity and a partial loss of protection against HX is formed along with U. In the kinetic unfolding experiments in 3 M GdnHCl monitored by HX-MS, an initial transient kinetic intermediate similar to I_E, with partial protection, is seen at early times of unfolding (Figure 4B). At later times of unfolding, I_E is not populated to a detectable extent (Figure 4B).

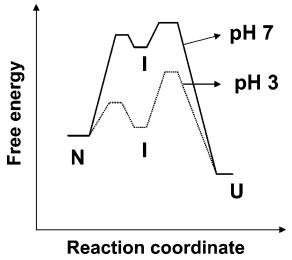

FIGURE 8: Stabilization of an unfolding intermediate at low pH. At pH 7, the barrier to unfolding is high, and the free energy diagram shows that the energy of the intermediate is too high for it to be detected. Unfolding therefore appears to be a two-state process. At pH 3, the barrier to unfolding is lowered. The free energy diagram shows that the stabilization of the transition state is accompanied by stabilization of I, which immediately precedes it on the reaction coordinate. U represents U_C which equilibrates slowly with U_T (see the text).

Thus, the unfolding of Trx at pH 3 can be represented as a $N \rightleftharpoons I \rightleftharpoons U$ system, where $I = I_1 \rightleftharpoons I_2 \rightleftharpoons I_E$, an ensemble of intermediates that are populated differentially at different GdnHCl concentrations in the range of 2.2−3 M. It seems possible to place I on the pathway between N and U because both the rates of formation and disappearance of its component I_2 can be measured in 2.2 and 2.3 M GdnHCl (Figure 6). It is seen that the rate of disappearance of I_2 is the same as the rate of formation of U. If I were off-pathway in an $I \rightleftharpoons N \rightleftharpoons U$ mechanism of unfolding, then I_2 would first have to refold for unfolding to occur. Such refolding will become slower with an increase in GdnHCl concentration. Since such a refolding step cannot be detected, it is likely that I_2 and, hence, I must be on-pathway.

Stabilization of an Unfolding Intermediate at Low pH. The unfolding studies at pH 7 and 3, reported here, indicate that the unfolding of Trx proceeds through a set of partially unfolded intermediates, I, which are stable and hence populated at pH 3 but unstable and hence not populated at pH 7. Moreover, the slow unfolding phase is faster at the lower pH, indicating that the transition state too is stabilized at low pH. This result suggests that the intermediate and transition state are either stabilized by an electrostatic interaction present only at pH 3 or destabilized by a repulsive electrostatic interaction present only at pH 7. The pI of Trx is 4.5, and the effect of pH may be only through its effect on the net charge on the protein, which in turn may influence electrostatic interactions present in the native, intermediate, and transition states. In the case of the folding of several other proteins, including hisactophilin (*60*), cro repressor (*61*, *62*), protein G (*63*), and the immunity proteins (*64*), a change in pH has been shown to stabilize folding intermediates and to cause a switch from apparent two-state folding to three-state folding. Here, a change in pH has been shown to stabilize an intermediate on the unfolding pathway of Trx and to cause a switch from apparent two-state unfolding to three-state unfolding.

Figure 8 shows free energy diagrams illustrating the mechanism of unfolding of Trx at pH 7 and 3. The transition state for the unfolding reaction (to U_C) is stabilized at pH 3 relative to that at pH 7; hence, the structural unfolding transition at pH 3 occurs 10 times faster at pH 3 than it does at pH 7. Not surprisingly, the stabilization of the transition state with the lowered pH is accompanied by a stabilization of an intermediate, I, that immediately precedes the transition state on the unfolding reaction pathway. At pH 3, this intermediate is seen to be populated at equilibrium at concentrations of GdnHCl in the range of 2.2−2.8 M, and it is seen to be populated transiently during the unfolding process at 3 M GdnHCl.

Transient Aggregation during Unfolding. In this study, it has been shown that the unfolding of Trx is decelerated at higher protein concentrations at pH 3, but not at pH 7. Since the native protein does not aggregate at either pH, it appears that the form of the protein that aggregates is partially unfolded intermediate I, which is populated at pH 3 but not at pH 7. The transient aggregation process during unfolding can be depicted as

$$\begin{array}{ccccc} N & \rightarrow & [I] & \rightarrow & U \\ & & \Updownarrow & & \\ & & I_A & & \end{array}$$

Since the rate and extent of aggregation of I will be dependent on protein concentration, the overall rate of unfolding will be expected to decrease at high protein concentrations. At low protein concentrations, transient aggregate I_A will not be populated significantly, and the unfolding rate will remain effectively invariant. At pH 7, the observed unfolding rate constant is independent of protein concentration because aggregate I_A does not form to any significant amount, as a result of I itself not being populated to a significant extent. In previous studies of the folding of several proteins, it had been shown that transient aggregation of folding molecules (*65*−*70*) may occur at high protein concentrations. Transient aggregation of intermediates that fold directly to native protein may decelerate folding (*69*, *70*). Here, it is shown that transient aggregation of an intermediate that directly unfolds to an unfolded protein can decelerate unfolding. The observation that transiently and partially unfolded intermediates can aggregate is important because of the presumption that native proteins are transformed into the amyloid fibrils that characterize many diseases, only after first unfolding transiently and partially (*71*).

ACKNOWLEDGMENT

We thank members of our laboratory for discussion and Kalyan Sinha for comments on the manuscript. Mass spectra were collected at the mass spectrometry facility at the National Centre for Biological Sciences.

REFERENCES

1. Segawa, S., and Sugihara, M. (1984) Characterization of the transition state of lysozyme unfolding. II. Effects of the intrachain crosslinking and the inhibitor binding on the transition state, *Biopolymers 23*, 2489−98.
2. Segawa, S., and Sugihara, M. (1984) Characterization of the transition state of lysozyme unfolding. I. Effect of protein-solvent interactions on the transition state, *Biopolymers 23*, 2473−88.
3. Zaidi, F. N., Nath, U., and Udgaonkar, J. B. (1997) Multiple intermediates and transition states during protein unfolding, *Nat. Struct. Biol. 4*, 1016−24.
4. Arrington, C. B., Teesch, L. M., and Robertson, A. D. (1999) Defining Protein Ensembles with Native-state NH Exchange: Kinetics of Interconversion and Cooperative Units from Combined NMR and MS Analysis, *J. Mol. Biol. 285*, 1265−75.

5. Leeson, L. T., Gai, F., Rodriguez, H. M., Gregoret, L. M., and Dyer, B. R. (2000) Protein folding and unfolding on a complex energy landscape, *Proc. Natl. Acad. Sci. U.S.A. 97*, 2527−32.
6. Juneja, J., and Udgaonkar, J. B. (2002) Characterization of the unfolding of ribonuclease a by a pulsed hydrogen exchange study: Evidence for competing pathways for unfolding, *Biochemistry 41*, 2641−54.
7. Sridevi, K., and Udgaonkar, J. B. (2003) Surface expansion is independent of and occurs faster than core solvation during the unfolding of barstar, *Biochemistry 42*, 1551−63.
8. Roy, M., and Jennings, P. A. (2003) Real-time NMR kinetic studies provide global and residue-specific information on the non-cooperative unfolding of the β-trefoil protein, interleukin-1β, *J. Mol. Biol. 328*, 693−703.
9. Wright, C. F., Lindorff-Larsen, K., Randles, L. G., and Clarke, J. (2003) Parallel protein-unfolding pathways revealed and mapped, *Nat. Struct. Biol. 10*, 658−62.
10. Hoeltzli, S. D., and Frieden, C. (1995) Stopped-flow NMR spectroscopy: Real-time unfolding studies of 6-19F-tryptophan-labeled *Escherichia coli* dihydrofolate reductase, *Proc. Natl. Acad. Sci. U.S.A. 92*, 9318−22.
11. Kiefhaber, T. (1995) Kinetic Traps in Lysozyme Folding, *Proc. Natl. Acad. Sci. U.S.A. 92*, 9029−33.
12. Phillips, C. M., Mizutani, Y., and Hochstrasser, R. M. (1995) Ultrafast thermally induced unfolding of RNase A, *Proc. Natl. Acad. Sci. U.S.A. 92*, 7292−6.
13. Konermann, L., Rosell, F. I., Mauk, A. G., and Douglas, D. J. (1997) Acid-Induced Denaturation of Myoglobin Studied by Time-Resolved Electrospray Ionization Mass Spectrometry, *Biochemistry 36*, 6448−54.
14. Sridevi, K., and Udgaonkar, J. B. (2002) Unfolding rates of barstar determined in native and low denaturant conditions indicate the presence of intermediates, *Biochemistry 41*, 1568−78.
15. Englander, S. W. (2000) Protein folding intermediates and pathways studied by hydrogen exchange, *Annu. Rev. Biophys. Biomol. Struct. 29*, 213−38.
16. Hamada, D., Segawa, S., and Goto, Y. (1996) Non-native α-helical intermediate in the refolding of β-lactoglobulin, a predominantly β-sheet protein, *Nat. Struct. Biol. 10*, 868−73.
17. Lakshmikanth, G. S., Sridevi, K., Krishnamoorthy, G., and Udgaonkar, J. B. (2001) Structure is lost incrementally during the unfolding of barstar, *Nat. Struct. Biol. 8*, 799−804.
18. Zocchi, G. (1997) Proteins unfold in steps, *Proc. Natl. Acad. Sci. U.S.A. 94*, 10647−51.
19. Oberhauser, A. F., Hansma, P. K., Carrion-Vazquez, M., and Fernandez, J. M. (2001) Stepwise unfolding of titin under force-clamp atomic force microscopy, *Proc. Natl. Acad. Sci. U.S.A. 98*, 468−72.
20. Dietz, H., and Rief, M. (2004) Exploring the energy landscape of GFP by single-molecule mechanical experiments, *Proc. Natl. Acad. Sci. U.S.A. 46*, 16192−7.
21. Mark, A. E., and Van Gusteren, W. F. (1992) Simulation of the thermal denaturation of hen egg white lysozyme: Trapping the molten globule state, *Biochemistry 31*, 7745−8.
22. Bryant, Z., Pande, V. S., and Rokhsar, D. S. (2000) Mechanical unfolding of a β-hairpin using molecular dynamics, *Biophys. J. 78*, 584−9.
23. Paci, E., Smith, L. J., Dobson, C. M., and Karplus, M. (2001) Exploration of partially unfolded states of human α-lactalbumin by molecular dynamics simulation, *J. Mol. Biol. 306*, 329−47.
24. Caughey, B., and Lansbury, P. T. (2003) Protofibrils, pores, fibrils, and neurodegeneration: Separating the responsible protein aggregates from the innocent bystanders, *Annu. Rev. Neurosci. 26*, 267−98.
25. Stefani, M., and Dobson, C. M. (2003) Protein aggregation and aggregate toxicity: New insights into protein folding, misfolding diseases and biological evolution, *J. Mol. Med. 81*, 678−99.
26. Ross, C. A., and Poirier, M. A. (2004) Protein aggregation and neurodegenerative disease, *Nat. Med. 10*, S10−7.
27. Chien, P., Weissman, J., and DePace, A. H. (2004) Emerging principles of conformation-based prion inheritance, *Annu. Rev. Biochem. 73*, 617−56.
28. Juneja, J., and Udgaonkar, J. B. (2003) NMR studies of protein folding. *Curr. Sci. 84*, 157−72.
29. Hoofnagle, A. N., Resing, K. A., and Ahn, G. N. (2003) Protein analysis by hydrogen exchange mass spectrometry, *Annu. Rev. Biophys. Biomol. Struct. 32*, 1−25.
30. Konermann, L., and Simmons, D. A. (2003) Protein-folding kinetics and mechanisms studied by pulse-labeling and mass spectrometry, *Mass Spectrom. Rev. 22*, 1−26.
31. Wales, E. T., and Engen, R. J. (2006) Hydrogen exchange mass spectrometry for analysis of protein dynamics, *Mass Spectrom. Rev. 25*, 158−70.
32. Miranker, A., Robinson, C. V., Radford, S. E., Aplin, R. T., and Dobson, C. M. (1993) Detection of transient protein folding populations by mass spectrometry, *Science 262*, 896−900.
33. Chung, E. W., Nettleton, E. J., Morgan, C. J., Gross, M., Miranker, A., Radford, S. E., Dobson, C. M., and Robinson, C. V. (1997) Hydrogen exchange properties of proteins in native and denatured states monitored by mass spectrometry and NMR, *Protein Sci. 6*, 1316−24.
34. Pan, H., and Smith, D. L. (2003) Quaternary structure of aldolase leads to differences in its folding and unfolding intermediates, *Biochemistry 42*, 5713−21.
35. Pan, H., Raza, A. S., and Smith, D. L. (2004) Equilibrium and kinetic folding of rabbit muscle triosephosphate isomerase by hydrogen exchange mass spectrometry, *J. Mol. Biol. 336*, 1251−63.
36. Zhang, Z., and Smith, D. L. (1993) Determination of amide hydrogen exchange by mass spectrometry: A new tool for protein structure elucidation, *Protein Sci. 2*, 522−31.
37. Katti, S. K., LeMaster, D. M., and Eklund, H. (1990) Crystal structure of thioredoxin from *Escherichia coli* at 1.68 Å resolution, *J. Mol. Biol. 212*, 167−84.
38. Maier, C. S., Schimerlik, M. I., and Deinzer, M. L. (1999) Thermal denaturation of *Escherichia coli* thioredoxin studied by hydrogen/deuterium exchange and electrospray ionization mass spectrometry: Monitoring a two-state protein unfolding transition, *Biochemistry 38*, 1136−43.
39. Kim, M. Y., Maier, C. S., Reed, D. J., and Deinzer, M. L. (2002) Conformational changes in chemically modified *Escherichia coli* thioredoxin monitored by H/D exchange and electrospray ionization mass spectrometry, *Protein Sci. 11* (6), 1320−9.
40. Kim, M. Y., Maier, C. S., Reed, D. J., and Deinzer, M. L. (2001) Site-specific amide hydrogen/deuterium exchange in *E. coli* thioredoxins measured by electrospray ionization mass spectrometry, *J. Am. Chem. Soc. 123*, 9860−6.
41. Kim, M. Y., Maier, C. S., Reed, D. J., Ho, P. S., and Deinzer, M. L. (2001) Intramolecular interactions in chemically modified *Escherichia coli* thioredoxin monitored by hydrogen/deuterium exchange and electrospray ionization mass spectrometry, *Biochemistry 40*, 14413−21.
42. Kelley, R. F., and Stellwagen, E. (1984) Conformational transitions of thioredoxin in guanidine hydrochloride, *Biochemistry 23*, 5095−102.
43. Kelley, R. F., Wilson, J., Bryant, C., and Stellwagen, E. (1986) Effects of guanidine hydrochloride on the refolding kinetics of denatured thioredoxin, *Biochemistry 25*, 728−32.
44. Kelley, R. F., and Richards, F. M. (1987) Replacement of proline-76 with alanine eliminates the slowest kinetic phase in thioredoxin folding, *Biochemistry 26*, 6765−74.
45. Georgescu, R. E., Li, J. H., Goldberg, M. E., Tasayco, M. L., and Chaffotte, A. F. (1998) Proline isomerization-independent accumulation of an early intermediate and heterogeneity of the folding pathways of a mixed α/β protein, *Escherichia coli* thioredoxin, *Biochemistry 37*, 10286−97.
46. Bhutani, N., and Udgaonkar, J. B. (2001) GroEL channels the folding of thioredoxin along one kinetic route, *J. Mol. Biol. 314*, 1167−79.
47. Bhutani, N., and Udgaonkar, J. B. (2003) Folding sub-domains of thioredoxin identified by native-state hydrogen exchange, *Protein Sci. 12*, 1719−31.
48. Agashe, V. R., and Udgaonkar, J. B. (1995) Thermodynamics of denaturation of barstar: Evidence for cold denaturation and evaluation of the interaction with guanidine hydrochloride, *Biochemistry 34*, 3286−99.
49. Reutimann, H., Straub, B., Luisi, P. L., and Holmgren, A. (1981) A Conformational Study of Thioredoxin and Its Tryptic Fragments, *J. Biol. Chem. 256*, 6796−803.
50. Perez-Jimenez, R., Godoy-Ruiz, R., Ibarra-Molero, B., and Sanchez-Ruiz, J. M. (2004) The efficiency of different salts to screen charge interactions in proteins: A Hofmeister effect, *Biophys. J. 86*, 2414−29.
51. Bai, Y., Milne, J. S., Mayne, L., and Englander, S. W. (1993) Primary structure effects on peptide group hydrogen exchange, *Proteins 17*, 75−86.

52. Kiefhaber, T., and Schmid, F. X. (1992) Kinetic coupling between protein folding and prolyl isomerization. I. Folding of ribonuclease A and ribonuclease T1, *J. Mol. Biol. 224*, 217−29.
53. Chandrasekhar, K., Krause, G., Holrngren, A., and Dyson, H. J. (1991) Assignment of the ^{15}N NMR spectra of reduced and oxidized *Escherichia coli* thioredoxin, *FEBS Lett. 284*, 178−83.
54. Dyson, H. J., Holrngren, A., and Wright, P. E. (1989) Assignment of the proton NMR spectra of reduced and oxidized thioredoxin: Sequence specific assignments, secondary structure, and global fold, *Biochemistry 28*, 7074−87.
55. Bolon, D. N., and Mayo, S. L. (2001) Polar residues in the protein core of *Escherichia coli* thioredoxin are important for fold specificity, *Biochemistry 40*, 10047−53.
56. Fox, R. O., Evans, P. A., and Dobson, C. M. (1986) Multiple conformations of a protein demonstrated by magnitization transfer NMR spectroscopy, *Nature 320*, 192−4.
57. Evans, P. A., Dobson, C. M., Kautz, R. A., Hatfull, G., and Fox, R. O. (1987) Proline isomerization in staphylococcal nuclease characterized by NMR and site directed mutagenesis. *Nature 329*, 266−8.
58. Pappenberger, G., Bachmann, A., Mullar, R., Aygun, H., Engels, J. W., and Kiefhaber, T. (2003) Kinetic mechanism and catalysis of a native-state prolyl isomerization reaction, *J. Mol. Biol. 326*, 235−46.
59. Reimer, U., and Fischer, G. (2002) Local structural changes caused by peptidyl−prolyl *cis*/*trans* isomerization in the native state of proteins, *Biophys. Chem. 96*, 203−12.
60. Houliston, R. S., Liu, C., Singh, L. M., and Meiering, E. M. (2002) pH and urea dependence of amide hydrogen-deuterium exchange rates in the β-trefoil protein hisactophilin, *Biochemistry 41*, 1182−94.
61. Laurents, D. V., Corrales, S., Elias-Arnanz, M., Sevilla, P., Rico, M., and Padmanabhan, S. (2000) Folding kinetics of phage 434 Cro protein, *Biochemistry 39*, 13963−73.
62. Sanchez, I. E., and Kiefhaber, T. (2003) Evidence for sequential barriers and obligatory intermediates in apparent two-state protein folding, *J. Mol. Biol. 325*, 367−76.
63. Park, S. H., Shastry, M. C., and Roder, H. (1999) Folding dynamics of the B1 domain of protein G explored by ultrarapid mixing, *Nat. Struct. Biol. 6*, 943−7.
64. Gorski, S. A., Capaldi, A. P., Kleanthous, C., and Radford, S. E. (2001) Acidic conditions stabilize intermediates populated during the folding of Im7 and Im9, *J. Mol. Biol. 312*, 849−63.
65. DeFelippis, M. R., Alter, L. A., Pekar, A. H., Havel, H. A., and Brems, D. N. (1993) Evidence for a self-associating equilibrium intermediate during folding of human growth hormone, *Biochemistry 32*, 1555−62.
66. Speed, M. A., Wang, D. I., and King, J. (1996) Specific aggregation of partially folded polypeptide chains: The molecular basis of inclusion body composition, *Nat. Biotechnol. 14*, 1283−7.
67. Pecorari, F., Minard, P., Desmadril, M., and Yon, J. M. (1996) Occurrence of transient multimeric species during the refolding of a monomeric protein, *J. Biol. Chem. 217*, 5270−6.
68. Raman, B., Ramakrishna, T., and Rao, C. M. (1996) Refolding of denatured and denatured/reduced lysozyme at high concentrations, *J. Biol. Chem. 271*, 17067−72.
69. Silow, M., and Oliveberg, M. (1997) Transient aggregates in protein folding are easily mistaken for folding intermediates, *Proc. Natl. Acad. Sci. U.S.A. 94*, 6084−6.
70. Ganesh, C., Zaidi, F. N., Udgaonkar, J. B., and Varadarajan, R. (2001) Reversible formation of on-pathway macroscopic aggregates during the folding of maltose binding protein, *Protein Sci. 10*, 1635−44.
71. Wetzel, R. (1996) For protein misassembly, it's the "I" decade, *Cell 86*, 699−702.

BI060647H